



Article

Complexity and Heterogeneity Evaluation of Pore Structures in the Deep Marine Shale Reservoirs of the Longmaxi Formation, China

Boyuan Zhu ^{1,2}, Jianghui Meng ^{1,*} , Chen Song ³, Renfang Pan ² , Zhengping Zhu ² and Jineng Jin ²

¹ Cooperative Innovation Center of Unconventional Oil and Gas, Yangtze University, Wuhan 430100, China; 2021730042@yangtzeu.edu.cn

² School of Geosciences, Yangtze University, Wuhan 430100, China; pan@yangtzeu.edu.cn (R.P.); 501096@yangtzeu.edu.cn (Z.Z.); jinjineng@yangtzeu.edu.cn (J.J.)

³ PetroChina Jidong Oilfield Company, Tangshan 063006, China; songchen2023@petrochina.com.cn

* Correspondence: mjh@yangtzeu.edu.cn

Abstract: The structural evolution and sedimentary differentiation of the Sichuan Basin in China are complex, with intricate reservoir pore structures that significantly impact shale gas production. This study examines the complexity and heterogeneity of the microscopic pore structures in the deep marine shale reservoir in the Longmaxi Formation. Pore structure characterization techniques are used to compare deep and shallow–medium marine shales, and siliceous and silty shales. The results reveal the factors influencing pore structure and their impact on exploration and development. The key points are as follows: (1) The pore structure of deep siliceous shale is the most complex due to its diverse range of pore development patterns, pore types, and sizes. (2) The box dimension of full pore size is about 1.52 for deep marine shale and 1.46 for shallow–medium shale. Organic matter (OM) content, the degree of pore development, and inorganic mineral content all correlate positively with the complexity of the pore structure in deep marine shale, which affects the formation of high-quality reservoirs. (3) Lateral heterogeneity of pore structures shows strong regional variations in the study area. Heterogeneity is more pronounced in the deep marine shale than in the medium and shallow shale formations. OM mesopores significantly influence the overall heterogeneity of the shale pore system. The deep marine shale reservoir is situated in an area with strong regional variations. The pore structure of high-quality reservoirs is more complex than those of shallow–medium marine shales, displaying notable heterogeneity. Pore structures with fractal dimension values close to that of the shallow–medium formations (box dimensions within 1.5) offer promising targets for the exploration and development of deep marine shale gas.

Keywords: Sichuan Basin; Longmaxi Formation; deep marine shale; pore structure; heterogeneity; fractal dimension



Citation: Zhu, B.; Meng, J.; Song, C.; Pan, R.; Zhu, Z.; Jin, J. Complexity and Heterogeneity Evaluation of Pore Structures in the Deep Marine Shale Reservoirs of the Longmaxi Formation, China. *J. Mar. Sci. Eng.* **2023**, *11*, 1613. <https://doi.org/10.3390/jmse11081613>

Academic Editor: George Kontakiotis

Received: 26 July 2023

Revised: 14 August 2023

Accepted: 16 August 2023

Published: 17 August 2023



Copyright: © 2023 by the authors. Licensee MDPI, Basel, Switzerland. This article is an open access article distributed under the terms and conditions of the Creative Commons Attribution (CC BY) license (<https://creativecommons.org/licenses/by/4.0/>).

1. Introduction

The surface micro-morphology and throat features of dual media pores have a major impact on the migration and accumulation of natural gas. Therefore, pore structures of shale reservoirs are an essential study topic for understanding shale gas enrichment [1,2]. Study of pore systems involves the characterization and analysis of heterogeneity, occurrence characteristics, evolution patterns, and the preservation mechanisms of pores [3–7].

Previous studies have found that organic matter (OM) pores (organic pores) in shale reservoirs are highly developed and complex [8,9]. OM abundance, thermal evolution level, diagenesis, and other factors combine in the creation and development of organic pores [10,11]. Other factors, including steric effects, the presence of hard minerals, and the morphology of the pores themselves, also affect the preservation and connectivity of organic pores [12–14]. Inorganic pores in shale reservoirs are mostly formed by brittle

minerals, and inorganic pores with complex structures can be observed under a scanning electron microscope [15,16]. As deeper shales experience more intense thermal evolution, a large number of pores are formed by thermal pyrolysis of OM. At the same time, strong compaction changes both organic and inorganic pores, resulting in relatively lower porosity and alteration of the original pore structure. The development of organic and inorganic pores together forms a complex pore system. The increased complexity and heterogeneity of the pore structures in deep marine shale reservoirs makes reservoir characterization more difficult [17,18]. This, in turn, increases the difficulty of evaluating the petrophysical properties, reservoir capacity, reservoir characteristics, and diageneses of reservoirs. Ultimately, these difficulties with reservoir interpretation can influence the results of shale gas transportation and enrichment. The complexity of pore structures also creates difficulties with reservoir geological modeling and petroleum engineering development [19–21].

The main research objects of this study are the deep and shallow–medium shales in the Luzhou, Weiyuan, and Changning regions. Field emission scanning electron microscopy (FE-SEM) and low-temperature gas adsorption were used to estimate the pore fractal dimension in order to analyze the complexity and heterogeneity of the pore structures. The comparative study highlighted the distinctions between deep marine shale and shallow–medium marine shale, and identified the key elements affecting the complexity and heterogeneity of pore networks in deep marine shale. The findings of this study provide a general theoretical basis for the evaluation and exploration of deep marine shale reservoirs.

2. Geological Setting

The main part of the Luzhou Block in the study area is in the southern Sichuan Basin's low folded structural belt. Its edges are in the gentle structural belt in the central part of the Sichuan Basin and the low folded structural belt in the southwestern part of the basin (Figure 1a) [22]. A comb anticline structure has developed from north to south in the Luzhou area, and several low and steep anticlines have developed in the northeast [23]. The thickness of shale in the Luzhou Block is fairly even across all of southern Sichuan [24].

The Longmaxi Formation lies at the base of the Lower Silurian System. Its lithology is primarily grayish-black and black rocks rich in silty shale, calcareous shale, and siliceous shale (Figure 1b). The formation thickness is between 200 and 500 m [24]. The Long₁ sub-member is the main formation for shale gas exploration and development, consisting of a set of deep-water shelf facies of organic-rich black shale divided into four sub-layers. The bottom of the Longmaxi Formation is a “sweet spot” formation formed of OM-rich siliceous shale covered with thick silty shale. Shale and tight limestone form the basement of the Wufeng Formation. Overall, the formation has good gas-bearing properties [25].

The deep black shale in the Luzhou area is predominantly silty shale and siliceous shale, with calcareous shale rarely occurring (Figure 1b). Calcareous shales are occasionally found in horizontal layered structures, with carbonatite mineral content generally ranging from 25% to 50% and low total organic carbon (TOC) content. Silty shales generally have a terrestrial brittle mineral content of 60% or less, horizontal layered structures, and low TOC content. The siliceous shale features horizontal bedding and siliceous nodules, with siliceous content exceeding 50% and TOC content generally exceeding 3%. It is rich in biological fossils.

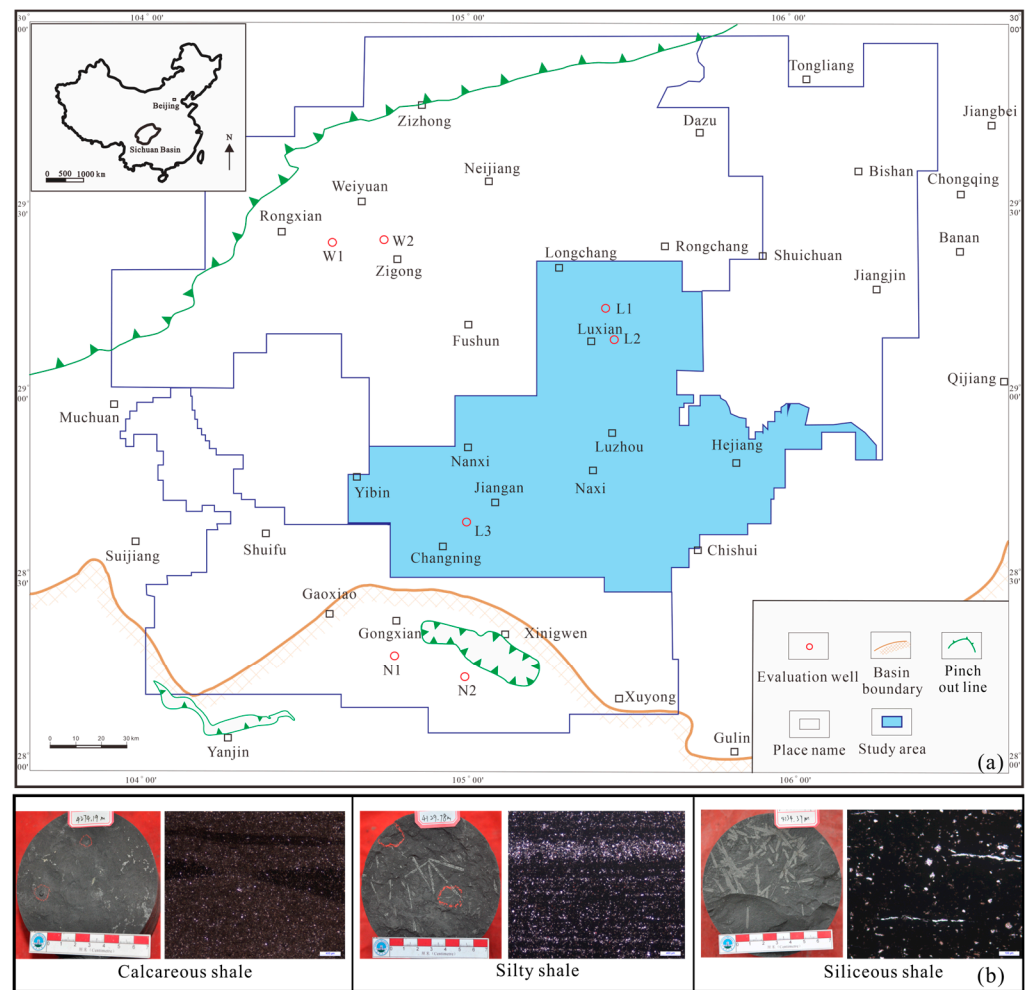


Figure 1. Overview of the study area in the southern Sichuan Basin. (a) Overview of the location of the study area; (b) common lithofacies of deep marine shale: core and thin rock sections.

3. Samples and Methods

3.1. Sample Data

The scope of current large-scale exploration for shale gas in the Sichuan Basin of China includes shallow shale (burial depth less than 2000 m), shallow–medium shale (burial depth between 2000–3500 m), and deep shale (burial depth between 3500–4500 m). In this study, a total of 16 core samples were analyzed to characterize the pore structure. Eleven samples were obtained from deep formations at approximately 4000 m burial depth in Luzhou and five from shallow–medium formations at around 2000 m burial depth in Changning and Weiyuan (Figure 1a). The sample set comprised 12 deep and shallow–medium siliceous shale formation samples, 3 deep silty shale samples, and 1 deep clay siliceous shale sample. The siliceous shale found in the Longmaxi Formation serves as a high-quality reservoir facies. Compared with other lithologies, it has relatively high TOC, brittle mineral content, porosity, and gas content [26].

SEM observations, nitrogen (N₂) and carbon dioxide (CO₂) adsorption experiments, tests of physical properties, organic geochemistry, and mineral X-ray diffraction were conducted on 16 samples, and model calculation and statistical analysis were carried out.

3.2. FE-SEM Observations

The instruments used for FE-SEM analysis were a Leica RES102 ion polishing instrument and a ZEISS high-resolution FE-SEM. FE-SEM is a kind of high-resolution scanning electron microscope, which is capable of secondary electron imaging, reflective electron

imaging, and image processing of the surface morphology of solid samples. The Zeiss FE-SEM produces high-resolution, high-quality images and has a large magnification range and strong stereoscopic imaging capability. Therefore, it is widely used in the characterization of microscopic pore structures. During initial pretreatment, millimeter-scale shale samples were subjected to argon ion polishing of their entire surfaces with an ion polisher. This made it easier to observe the nanoscale pore structure of the shale.

In observing images at different positions along a certain direction using FE-SEM, it is necessary to use an electron gun to emit an electron beam and focus it on the surface of the shale sample while sequentially scanning the sample surface row by row. Secondary electrons emitted from the sample surface are then collected from the monitor. The image signal formed by these electrons is displayed by a cathode ray tube (CRT). In order to keep the position of the sample image displayed by the CRT consistent with the position of the electron beam on the sample surface, the deflection coil of the CRT must be synchronized with the scanning coil.

To accurately quantify the information captured in the SEM images, threshold segmentation of each photo was first performed, converting the entire image to 8-bit grayscale. Subsequently, useful data, such as the OM area, were extracted based on the grayscale values. Finally, 8 to 10 images of each sample with a magnification of around 10 to 20 K were randomly selected for statistical analysis. The statistical results of all images for each individual sample were then collated to obtain data for that sample.

3.3. Low-Temperature Gas Adsorption Method

In N₂ adsorption experiments, based on the BET (Brunauer–Emmett–Teller) theory, the shale specific surface area (SSA) was determined at relative pressures (P/P_0) ranging from 0.05 to 0.35 MPa [27]. Equivalent pore volumes (PVs) were obtained using the BJH (Barrett–Joyner–Halenda) model [28]. N₂ adsorption was used to determine the pore size distribution of mesopores (pore sizes 2–50 nm).

CO₂ molecules have higher adsorption temperatures than N₂, resulting in more vigorous thermal motion. At 0 °C, the saturated vapor pressure of CO₂ reaches 3.495 MPa, making it easier for CO₂ molecules to diffuse into micropores (pore size less than 2 nm) in rock samples. The PV and SSA of micropores can be estimated using the DFT (Density Functional Theory) model [29].

3.4. Estimation of Fractal Dimension

Two-dimensional fractals of pores can be approximated using the SEM-box-counting method, while three-dimensional fractals of pores can be approximated using the Frankel–Halsey–Hill (FHH) theory [30,31].

The box dimension is calculated using the connection between the number of boxes and their sizes [32]. By adjusting the threshold and particle size of the SEM grayscale, the fractal dimensions of different pore sizes can be estimated [8]. The box’s dimensions are as follows:

$$D_B = -\lim_{\delta \rightarrow 0} \frac{\log N_\delta}{\log \delta} \tag{1}$$

where N_δ is the number of boxes required to cover the material each time, and δ is the box size (nm). The logarithmic relationship between N_δ and δ is established as follows:

$$\log N_\delta = -D_B \log \delta + c \tag{2}$$

where the absolute value of the slope is the box-counting dimension D_B , and C is a constant. D_{B1} is the box dimension of mesopores, with pore sizes of 10–50 nm; D_{B2} is the box dimension of macropores; D_{B3} is the box dimension of the full range of pore sizes in the FE-SEM images.

The branch of the N₂ adsorption–desorption curve in the low-pressure area (relative pressure less than 0.45) corresponds to pores with diameter less than 4.34 nm and its

fractal dimension is D_1 [29]. The branch of the N_2 adsorption–desorption curve in the high-pressure zone corresponds to 4.34–100 nm pores with relative pressure greater than 0.45, and the fractal dimension is D_2 [33]. The FHH fractal dimension is as follows:

$$\ln V = (D - 3)\ln[(P_0/P)] + c^2 \quad (3)$$

where V is the volume of adsorbed gas, m^3 ; P_0 is saturated vapor pressure, MPa; and p is equilibrium pressure (MPa).

4. Results

4.1. FE-SEM Pore Characteristics

Different lithofacies in shale samples from the deep and shallow–medium marine shale were observed in FE-SEM images (Figure 2). Figure 2a–c show that organic pores are the most developed in deep siliceous shale and that the pores in shallow–medium siliceous shale are the same as those in deep silty shale. Figure 2d–f show that the organic pores of the deep and shallow siliceous shale have high densities of mesopores, while the deep silty shale has a relatively low density of mesopores but a relatively high density of macropores (pore size greater than 50 nm). The organic mesopores and macropores are all irregular; however, macropore structures are more complex. Figure 2g–i show that inorganic pores are not very developed in the deep silty shale, deep siliceous shale, and shallow–medium siliceous shale, as shown by the complex structure of fractures and angular pores. The FE-SEM images reveal that the pore network distribution of the deep siliceous shale has the highest density.

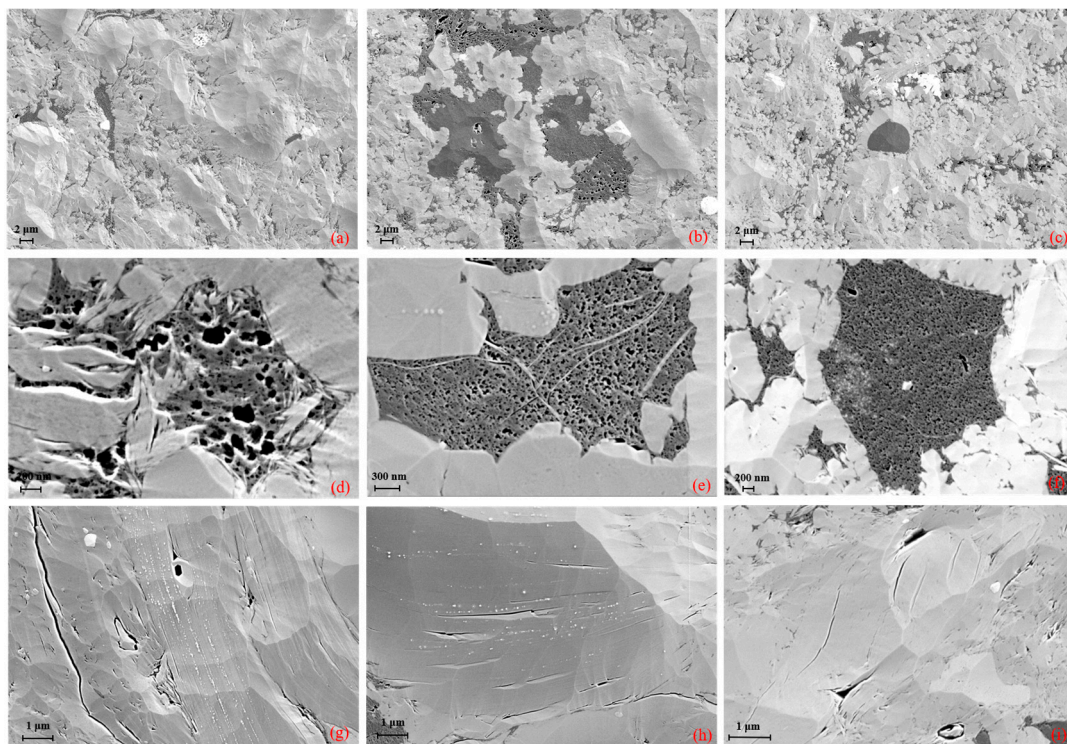


Figure 2. FE-SEM pore characteristics of shale samples in the study area. (a) Sample L1-1, 4126 m, pore distribution of silty shale; (b) sample L1-4, 4144 m, pore distribution of siliceous shale; (c) sample N1-2, 2317 m, pore distribution of siliceous shale; (d) sample L1-1, 4126 m, silty shale with developed organic pores; (e) sample L1-6, 4149 m, siliceous shale with developed organic pores; (f) sample N1-3, 2322 m, siliceous shale with developed organic pores; (g) sample L1-1, 4126 m, silty shale with developed inorganic pores; (h) sample L1-6, 4149 m, siliceous shale with developed inorganic pores; (i) sample N1-1, 2581 m, silty shale with developed inorganic pores.

The pores in the SEM images were statistically analyzed to determine surface porosity. The inorganic surface porosity of deep marine shale is the highest while the formation of organic pores is controlled by lithofacies (Figure 3 gray). The organic surface porosity of the siliceous shale is the highest and that of the deep marine shale is higher than that of the shallow–medium marine shale (Figure 3 yellow). According to surface porosity characteristics, deep siliceous shale has the most developed organic and inorganic pores.

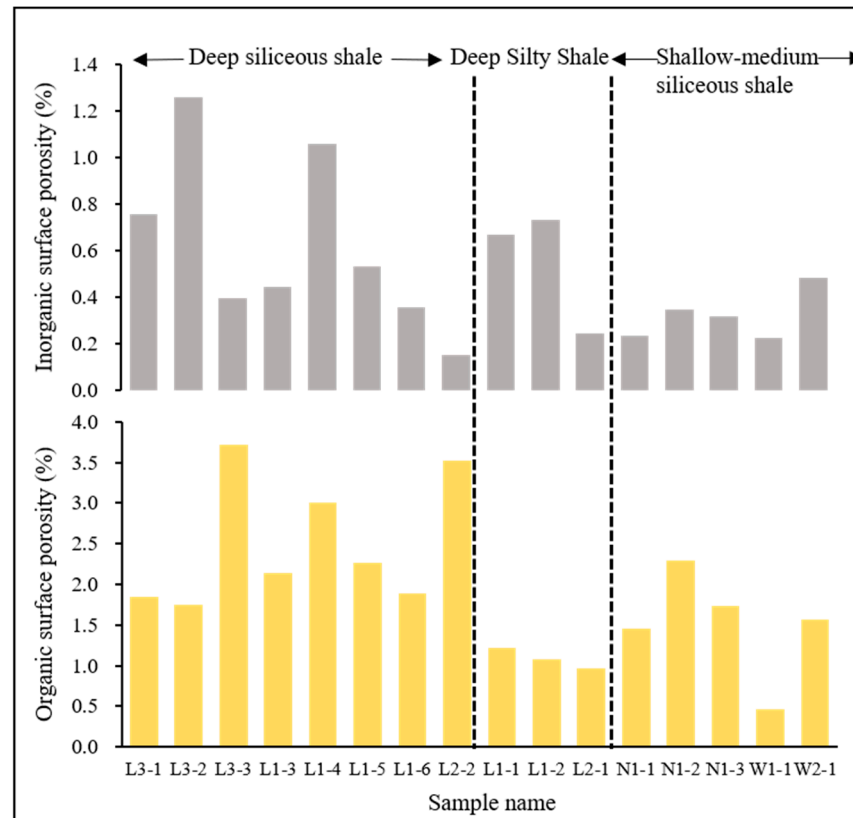


Figure 3. Pore surface porosity based on FE-SEM.

4.2. N₂ Adsorption–Desorption Characteristics

The hysteresis loop characteristics (H1–H4 types) were defined according to IUPAC [34]. Figure 4 shows that the adsorption curves of all samples show a gradual increase in the low-to-medium-pressure range (0–0.8) and a steep incline in the high-pressure range (0.8–1.0), which is typical H3 type behavior. However, deep siliceous shale samples, specifically L-5 and L-6, have wider hysteresis loops with higher adsorption capacities, which is more typical of H2-type behavior. As a result, deep siliceous shale can be classified as a hybrid of H2 and H3 types, referred to here as H2&3 type, while the deep silty shale and shallow–medium marine shale fall within the H3 type.

The presence of the H2&3 type leads to a diverse range of pore characteristics and a decrease in pore connectivity within the rock. On the contrary, the H3-type pore structure appears to be comparatively simple and exhibits comparatively good pore connectivity.

The hysteresis loop of N₂ adsorption–desorption shows that the pores of deep siliceous shale are very developed and their pore structure is the most complex. However, the pore structure complexities of deep silty shale and shallow–middle siliceous shale are similar.

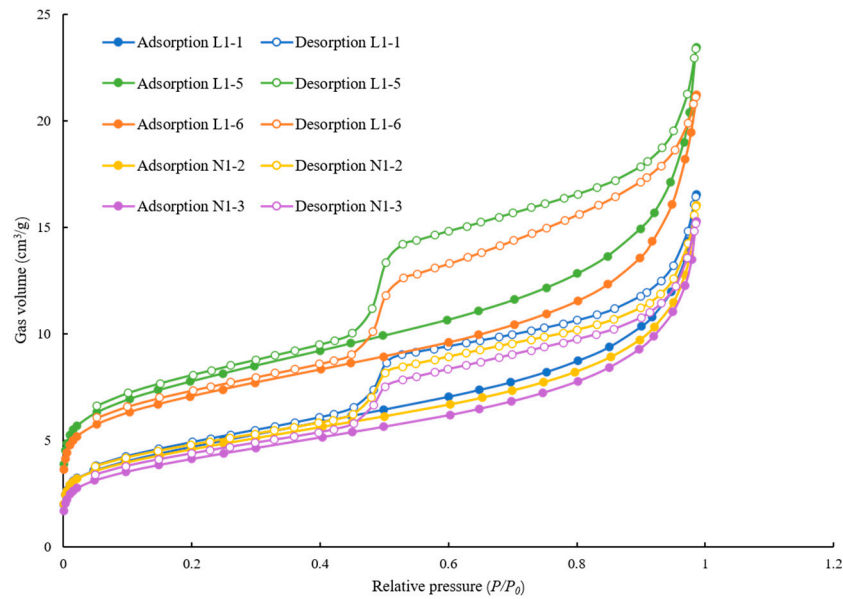


Figure 4. N₂ adsorption–desorption characteristics.

4.3. Pore Size Distribution

The full PV, and the SSA distribution, of each sample’s pore sizes can be estimated using the N₂ adsorption BJH model and CO₂ adsorption DFT model.

Figure 5 clearly shows that the mesopores in the shallow–medium siliceous shale contribute more to PV and SSA. In comparison with shallow–medium siliceous shale, the micropores and macropores in deep marine shale greatly increase the PV (Figure 5). Compared with the silty shale, the deep siliceous shale has more macropores (about 14%) (Figure 5).

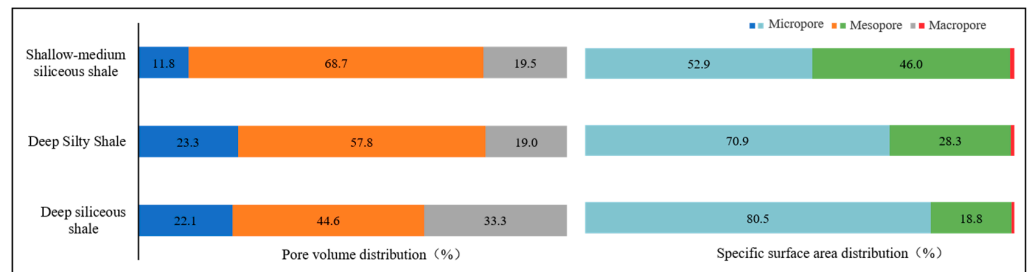


Figure 5. Distribution of PV and SSA proportion.

The variations in PV and SSA with different depths and lithologies reveal that the pore systems in deep marine shale formations are not dominated solely by mesopores. The contributions of micropores and macropores cannot be ignored. The contribution from macropores is more developed.

4.4. Fractal Characteristics of Pores

The complexity of the pore structures increases with the size of the fractal dimension. Box-counting based on SEM images indicates the complexity of the organic pore structure. D_{B1} of wells N1, W1, and W2 in the shallow–medium marine shale is higher than that in the deep marine shale, with an average absolute deviation of +0.16, while D_{B2} and D_{B3} are smaller than that in the deep marine shale (Table 1), with an average absolute deviation of −0.1 and −0.06, respectively. The box-counting dimension relationship between different lithofacies is not significant (Table 1). Analysis of the box-counting dimension reveals that the mesopore structure of the shallow–medium marine shale is more complex than that of the deep marine shale. Conversely, the macropore structure of the deep marine shale

is more complex. The organic pore structure of the deep marine shale is evidently more intricate than that of the shallow–medium marine shale.

Table 1. Sample box-counting dimension, FHH fractal dimension, and SEM average pore size.

Sample	Depth	Lithology	D_B			D		SEM Average Pore Size
	m		D_{B1}	D_{B2}	D_{B3}	D_1	D_2	nm
L1-1	4127	Silty shale	1.185	1.647	1.536	2.549	2.766	27.4
L1-2	4134	Silty shale	1.102	1.577	1.514	2.586	2.760	30.1
L1-3	4139	Siliceous shale	1.151	1.566	1.487	2.578	2.758	27.1
L1-4	4143	Siliceous shale	1.170	1.631	1.461	2.634	2.786	24.8
L1-5	4147	Siliceous shale	1.199	1.570	1.489	2.640	2.776	21.6
L1-6	4148	Siliceous shale	1.390	1.475	1.514	2.613	2.761	29.8
L3-1	3825	Siliceous shale	1.139	1.651	1.571	2.596	2.766	64.3
L3-2	3837	Siliceous shale	1.121	1.623	1.580	2.596	2.750	28.6
L3-3	3844	Siliceous shale	1.169	1.620	1.503	2.578	2.758	28.7
L2-1	4113	Silty shale	1.146	1.604	1.512	2.621	2.811	24.1
L2-2	4143	Siliceous shale	1.508	1.754	1.515	2.638	2.809	19.6
N1-1	2580	Siliceous shale	1.422	1.537	1.598	2.508	2.744	19.9
N1-2	2318	Siliceous shale	1.377	1.550	1.478	2.572	2.763	13
N1-3	2323	Siliceous shale	1.406	1.422	1.499	2.526	2.752	22.6
W1-1	1541	Siliceous shale	1.229	1.568	1.249	2.597	2.815	10.4
W2-1	2568	Siliceous shale	1.407	1.475	1.462	2.607	2.733	17.2

Pore structures are characterized based on their FHH fractal dimension. D_1 and D_2 of the shallow–medium marine shale are generally smaller than that of the deep marine shale (Table 1), with an average absolute deviation of -0.04 and -0.012 , respectively. Therefore, the pore structure of the deep marine shale is more complex than that of the shallow–medium marine shale. D_1 of the silty shale is small (-0.024 deviation), while the D_2 relationship is not significant (0.008) (Table 1). Therefore, the complexity of the different lithofacies is about the same.

Heterogeneity of Pore Structures

Examination of the fractal dimension across different pore sizes illustrates the heterogeneity of the shale pore system. As shown in Table 1, the fractal dimension varies significantly between different pore sizes. Micropores have a comparatively simple structure, characterized by the smallest fractal dimension [35]. The wide range of variations in the fractal dimension of all the pore sizes in the pore system demonstrates the considerable heterogeneity of the overall pore system.

It is also worth noting that the fractal dimension of full pore size in deep marine shale formations is higher than that in the shallow–medium marine shale (Table 1). This indicates that heterogeneity is more pronounced in the pore system of the deep marine shale of the Longmaxi Formation than in the shallow–medium marine shale.

Variations in the box-counting dimension based on FE-SEM images represent the horizontal and vertical heterogeneity of organic pore structures. Figure 6 shows that the organic pore heterogeneity in Luzhou, Changning, and Weiyuan is strong. The D_{B3} heterogeneity of organic pores in the shallow–medium marine shale is stronger than that in the deep marine shale, and the difference in heterogeneity between siliceous shale and silty shale is not significant (Figure 6). Figure 6 shows that the D_{B3} organic pore heterogeneity over the entire vertical depth range is comparatively weak. The most drastic changes in either the horizontal or vertical directions occur in D_{B1} . Overall heterogeneity of the pore structure is influenced by the heterogeneity of organic mesopores.

Variation in the FHH fractal dimension is used to characterize the horizontal and vertical heterogeneity of pore structures. Figure 7 shows strong horizontal heterogeneity of D_1 and D_2 in the pore structures of Luzhou, Changning, and Weiyuan. The difference in heterogeneity across the shallow–medium marine shale is not obvious, and the difference in heterogeneity between siliceous shale and silty shale is also not obvious (Figure 7). Figure 7 shows that the vertical homogeneity of pore structures at depth D_2 is comparatively good.

The difference in heterogeneity across shallow–medium and deep marine shale formations is not obvious. D_1 changes most drastically in both horizontal and vertical directions.

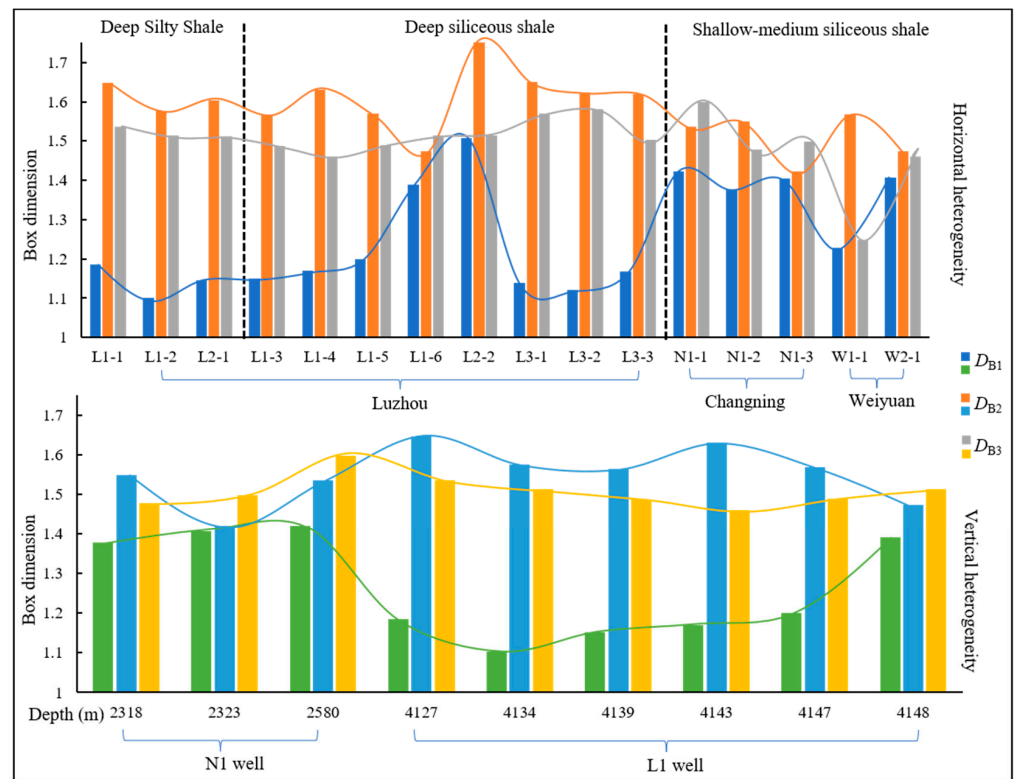


Figure 6. Heterogeneity of organic pore structure based on box dimension.

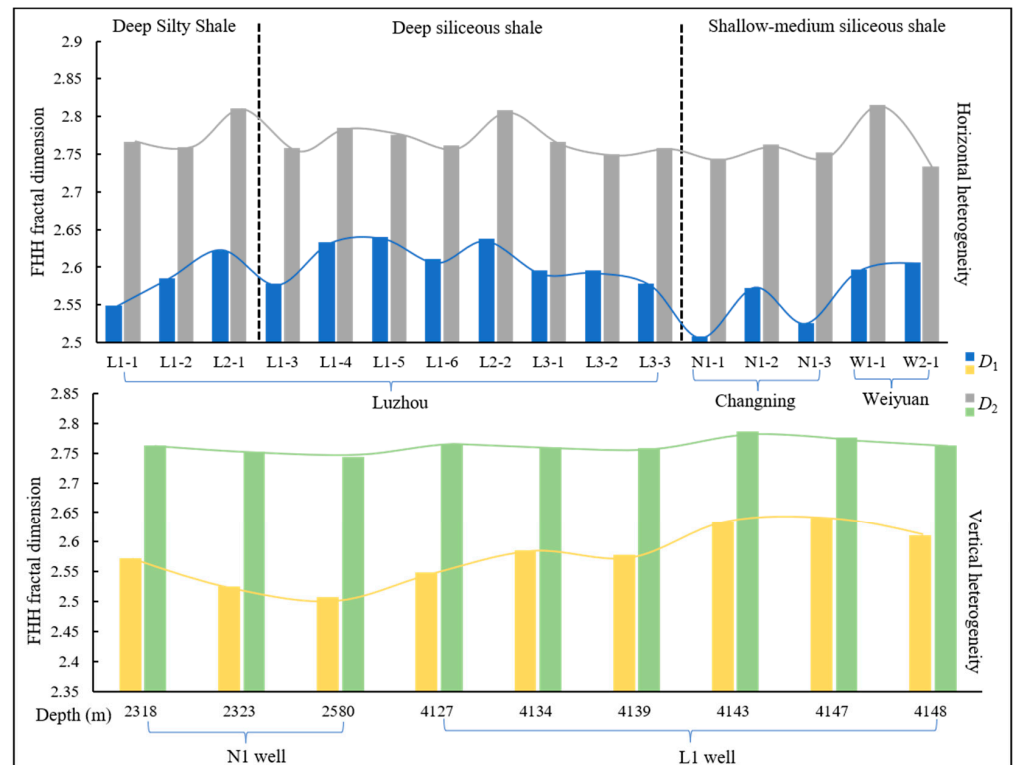


Figure 7. Heterogeneity of pore structure based on FHH fractal dimension.

5. Discussion

5.1. Factors Influencing Pore Structure Complexity

5.1.1. Influencing Factors

The FHH fractal dimension represents the degree of complexity of the pore network. Figure 8 illustrates the relationship between reservoir parameters and fractal dimension after excluding outliers.

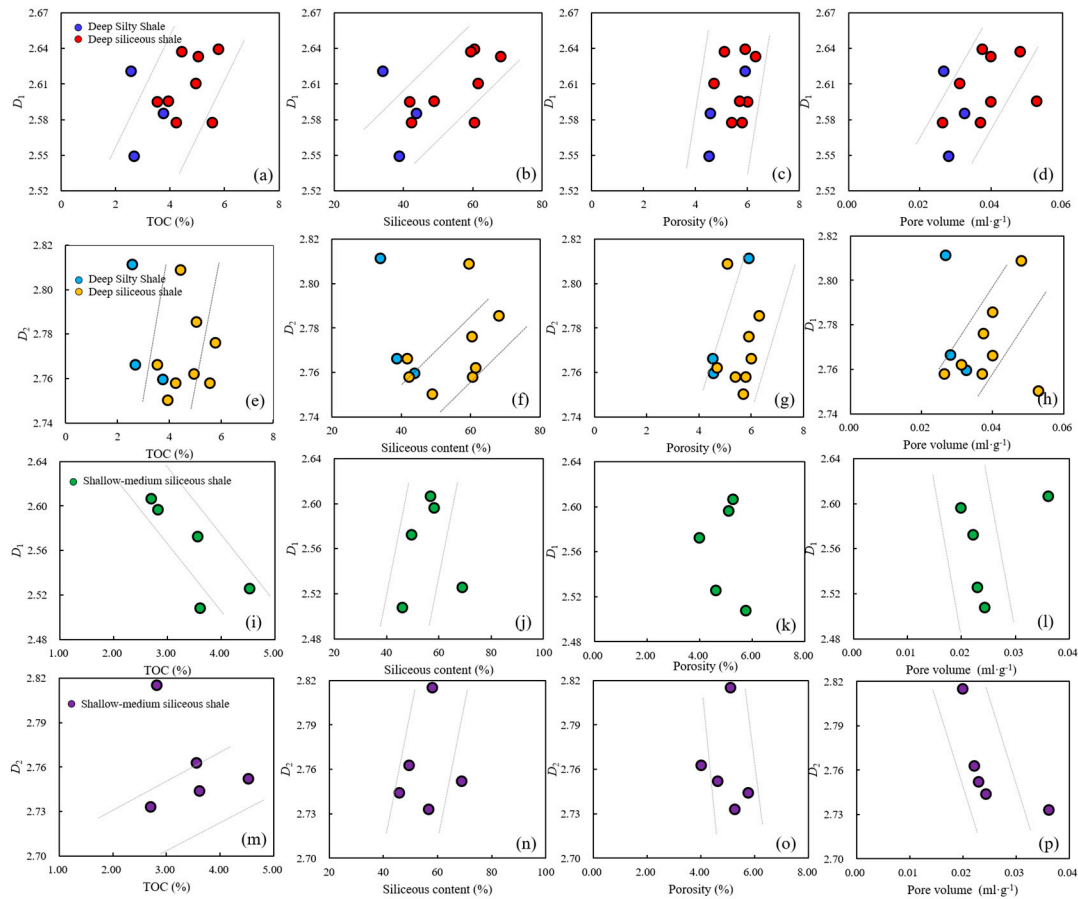


Figure 8. Relationship between fractal dimension and reservoir parameters. (a–d) The relationship between deep marine shale D_1 and TOC, siliceous content, porosity, and PV; (e–h) the relationship between deep marine shale D_2 and TOC, siliceous content, porosity, and PV; (i–l) the relationship between shallow–medium marine shale D_1 and TOC, siliceous content, porosity, and PV; (m–p) the relationship between shallow–medium marine shale D_2 and TOC, siliceous content, porosity, and PV.

It can be observed from Figure 8a–d that D_1 of the deep marine shale is positively correlated with TOC, siliceous content, porosity, and PV. Figure 8e–h show that D_2 of the deep siliceous shale is still positively correlated with reservoir parameters. This relationship indicates that the degree of pore development, the amounts of inorganic minerals, and the quantity of OM all have a significant impact on the complexity of the pore structure of deep marine shale.

Figure 8i–l show that D_1 of the shallow–medium siliceous shale is positively correlated with siliceous content to a considerable degree but negatively correlated with TOC and PV. Figure 8m–p show that D_2 of the shallow–medium siliceous shale is positively correlated with TOC and siliceous content but negatively correlated with porosity and PV. This indicates that the complexity of small pores in the shallow–medium marine shale is influenced by the content of inorganic minerals and the degree of pore development. The quantity of OM and the presence of inorganic minerals both affect the complexity of larger pores in the shallow–medium marine shale.

In summary, more factors contribute to the complexity of the pore structure of deep marine shale than to the shallow–medium layers, resulting in a more complex pore structure in the deep marine shale (Table 1). Deep siliceous shale may also be influenced by more factors than silty shale.

5.1.2. Formation of Influencing Factors

The growth of organic pores and their structural characteristics are directly tied to TOC and may be significantly impacted by both the place of origin and quantity of OM [36]. Moreover, the content of siliceous minerals can influence the development and structure of inorganic pores. Also, the interaction between rigid minerals and OM can cause pores to form under high pressure, generating elongated intergranular pores (Figure 2e). The porosity and PV directly reflect the overall degree of pore development.

(1) Organic matter: The overall results show that the complexity of the pore structure of the deep marine shale is controlled by organic matter (Figures 3 and 4; Table 1). The deep marine shale has undergone high levels of thermal evolution and compaction. Hydrocarbon production is beneficial for the formation of organic matter pores, while compaction has a negative effect. The combination of these two processes results in a highly complex structure of organic pores. Additionally, during its sedimentary period, the “sweet spot” interval of the Longmaxi Formation in the Luzhou area was located at the center of deposition, where the water depth was greatest. In contrast, the Changning and Weiyuan areas were located on slopes, leading to differences in OM sources between the two areas [37,38]. Therefore, there is a certain difference in the degree to which the abundance of deep and shallow organic matter controls the complexity of pores.

(2) Inorganic mineral content: Complex inorganic pores (commonly macropores) tend to develop with increasing content of inorganic minerals. If rigid mineral particles are in a dispersed state and do not come into contact with each other, they can compress the organic matter, leading to the destruction of organic pores [39]. Intergranular pores formed by extrusion between inorganic minerals and organic matter have worse storage and connectivity compared with organic pores [40]. Inorganic mineral content and contact relationships of rigid minerals are influential factors in the complexity of inorganic and organic pores in shale reservoirs.

(3) Pore development degree: Compared with the shallow–medium marine shale, the deep marine shale exhibits substantial organic pore development (Figures 2 and 3). The extensive development of organic pores has a substantial impact on the intricate nature of the pore structure seen in deep marine shale formations. The organic pores in the deep marine shale have highly developed micropores, mesopores, and macropores (Figure 5), and both organic and inorganic pores have comparatively high surface porosity (Figure 3). Increased pore development implies more diverse origins for the pore components. In contrast, the shallow–medium marine shale is primarily composed of mesopores. As the degree of pore development in these shales increases, the complexity of the pore structure decreases.

Broadly speaking, organic matter in deep marine shale undergoes substantial thermal evolution and compaction [41,42], leading to an abundance of irregular organic pores. At the same time, destruction of inorganic primary pores and formation of inorganic secondary pores also occur, resulting in a very complex pore structure. As suggested by the distribution of full-size PV contributions and fractal dimension characteristics, this pattern of pore development means that the pore structure of deep marine shale is the most complex. In the Luzhou area, the full-size pores in the deep marine shale are widely dispersed, a phenomenon also observed in the Dazu and Yongchuan areas [43]. In contrast, shallow–medium marine shales typically have widely developed mesopores. The pore structure of deep marine shale is, therefore, more complicated than that of shallow–medium marine shale because pore structures become simpler as pore size decreases.

5.2. Impact of Heterogeneity and Complexity on Exploration

5.2.1. Heterogeneity and Complexity of Reservoir Pore Structures

The Box-counting dimension and FHH fractal dimension serve as crucial parameters for characterizing the heterogeneity of pore structures, as they accurately reflect their complexity and are helpful for identifying factors that contribute to the intricacy of these structures.

The heterogeneity of the deep marine shale pore system is stronger than that of the shallow–medium shale, and the entire shale pore structure has strong lateral heterogeneity. The primary reason for this is the continuous alteration of organic mesopores in shale, as they are transformed into micropores under compaction and into macropores during hydrocarbon generation [44,45]. The heterogeneity of organic mesopores is highly pronounced, leading to a lack of uniformity in pore structures (Figures 6 and 7).

TOC, porosity, brittle mineral content (including siliceous content), and PV are important factors in the classification and evaluation of high-quality shale reservoirs in the Longmaxi Formation. Increases in their values mean that the shale reservoir capacity has improved. The FHH fractal dimension of the deep siliceous shale directly correlates with TOC, porosity, siliceous content, and PV, influenced by a wider range of factors than in the shallow–medium marine shale. Consequently, the better the quality of the deep marine shale reservoir, the more complex the pore structure becomes. Simultaneously, the heterogeneity of the pores, which is influenced by complexity, is also an important factor to be taken into consideration.

5.2.2. Implications for Exploration

A strong shale oil and gas generation base exists in the deep marine shale of the Longmaxi Formation in southern Sichuan [46]. However, our results indicate strong regional specificity of the reservoir. The pore structure of high-quality reservoirs is more complex than in the shallow–medium marine shale, with pronounced heterogeneity in the pore system. A certain degree of heterogeneity in storage space is necessary for effective natural gas storage; however, an overly complex pore structure is not conducive to extraction.

Exploitation of deep marine shale reservoirs is a serious challenge. Clarifying the main influencing factors of pore structure complexity and heterogeneity in deep marine shale will enable us to evaluate and distinguish complex pore space more easily. Further, the reservoir type can be more finely judged. In addition, targeted improvement of organic pore structure may enhance the reservoir's permeability and storage capacity in the future. Therefore, study of the complexity and heterogeneity of pore structures is of great significance for China's drive to commercially exploit deep marine shale gas. For the Longmaxi Formation's deep marine shale reservoir, selecting targets with fractal dimension values close to those of shallow–medium marine shale is a promising direction for deep marine shale gas exploration and development.

6. Conclusions

Deep shale is enriched with a variety of types of organic matter, influenced by thermal evolution, compaction, and mineral contact relationships, leading to development of irregular organic pores. In addition, complex inorganic pore development occurs, resulting in highly complex pore structures in deep marine shale. FE-SEM and fractal dimension do not fully characterize smaller micropores structures; so, the complexity of these pores needs to be further verified by experiments.

Patterns of pore development contribute to the complexity of deep marine shale pore structures. Pores in deep marine shale are widely dispersed and pore sizes are distributed across the entire pore size range, increasing the complexity of both pore types and sizes. However, the shallow–medium marine shale predominantly contains mesopores, so the structure is comparatively simple.

The complexity of deep siliceous shale pore structures is correlated with the abundance of OM, the degree of pore development, and inorganic mineral content. These factors also affect the formation of high-quality reservoirs. Comparatively fewer factors influence the pore structures in deep silty shale and shallow–medium siliceous shale.

Evaluation of lateral heterogeneity in pore structures highlights the strong regional variations in the study area. The heterogeneity of deep marine shale pore systems surpasses that of shallow–medium marine shale. Therefore, the heterogeneity of shale pore systems is largely determined by organic mesopores.

The higher the quality of a deep marine shale reservoir, the more complex the pore structure becomes. At the same time, the pore structures in high-quality reservoirs have strong heterogeneity, which presents challenges for reservoir exploration and development.

Author Contributions: B.Z.: Conceptualization, sorting out ideas, and writing—original draft. J.M.: Writing—review and editing, funding acquisition, and sorting out ideas. R.P.: Writing—review and editing. C.S.: Writing—review and editing, investigation. Z.Z.: Writing—review and editing, investigation. J.J.: Writing—review and editing, investigation. All authors have read and agreed to the published version of the manuscript.

Funding: This research is supported by the Youth Project of the National Natural Science Foundation of China (No. 41402114) and the Outstanding Young and Middle-aged Scientific and Technological Innovation Team Plan Project of Colleges and Universities in Hubei Province (No. t201905).

Institutional Review Board Statement: Not applicable.

Informed Consent Statement: Not applicable.

Data Availability Statement: The data presented in this study are available on request from the corresponding author.

Acknowledgments: The authors would like to thank PetroChina Southwest Oil & Gas field Company.

Conflicts of Interest: The authors declare no conflict of interest.

References

- Han, K.; Ju, Y.; Wang, G.; Bao, S.; Bu, H.; Neupane, B. Shale composition and pore structure variations in the progradation direction A case study of transitional shales in the Xu-Huai district, Southern North China. *J. Nat. Gas Sci. Eng.* **2016**, *36*, 1178–1187. [[CrossRef](#)]
- Wang, S.; Li, J.; Lu, S.; Zhang, P.; Zhang, J.; Zhang, W. Development characteristics of organic matter pores of marine shale in the Southeastern Chongqing, China. *J. Earth Sci. Environ.* **2019**, *41*, 721–733.
- Mahjour, S.K.; Correia, M.G.; Santos, A.; Schiozer, D.J. Developing a workflow to represent fractured carbonate reservoirs for simulation models under uncertainties based on flow unit concept. *Oil Gas Sci. Technol.* **2019**, *74*, 15. [[CrossRef](#)]
- Duan, W.; Lin, W.; Tian, J.; Ma, J.; Du, M.; Luo, J. Fractal characteristics and main controlling factors of Wufeng-Longmaxi Formation shale in Luobu Syncline, Southern Sichuan Basin. *Xinjiang Pet. Geol.* **2022**, *43*, 153–159.
- Wu, S.; Zhu, R.; Cui, J.; Cui, J.; Bai, B.; Zhang, X.; Jin, X.; Zhu, D.; You, J.; Li, X. Characteristics of lacustrine shale porosity evolution, Triassic Chang 7 Member, Ordos Basin, NW China. *Pet. Explor. Dev.* **2015**, *42*, 167–176. [[CrossRef](#)]
- Zhang, K.; Song, Y.; Jia, C.; Jiang, Z.; Han, F.; Wang, P.; Yuan, X.; Yang, Y.; Zeng, Y.; Li, Y.; et al. Formation mechanism of the sealing capacity of the roof and floor strata of marine organic-rich shale and shale itself, and its influence on the characteristics of shale gas and organic matter pore development. *Mar. Pet. Geol.* **2022**, *140*, 105647. [[CrossRef](#)]
- Liu, S.; Jiao, K.; Zhang, J.; Ye, Y.; Xie, G.; Deng, B.; Ran, B.; Li, Z.; Wu, J.; Li, J.; et al. Research progress on the pore characteristics of deep shale gas reservoirs: An example from the Lower Paleozoic marine shale in the Sichuan Basin. *Nat. Gas Ind.* **2021**, *41*, 29–41.
- Zhu, B.; Meng, J.; Pan, R.; Hu, H.; Song, C.; Zhu, Z.; Jin, J. New insights into the evaluation criteria for high-quality deep marine shale gas reservoirs in the Longmaxi formation: Evidence from organic matter pore development characteristics. *Front. Ecol. Evol.* **2023**, *11*, 1138991. [[CrossRef](#)]
- Li, Y.; Liu, X.; Cai, C.; Hu, Z.; Wu, B.; Mu, Y.; Duan, X.; Zhang, Q.; Zeng, S.; Guo, J.; et al. Pore Structure Characteristics and Their Controlling Factors of Deep Shale: A Case Study of the Lower Silurian Longmaxi Formation in the Luzhou Area, Southern Sichuan Basin. *ACS Omega* **2022**, *7*, 14591–14610. [[CrossRef](#)]
- Sun, L.; Fu, D.; Wu, Y.; Wang, Z. The current study and development of organic matter pores in organic-rich shale. *Arab. J. Geosci.* **2022**, *15*, 62. [[CrossRef](#)]
- Barry, J.K.; Irene, A. Organic porosity: A geochemist's view of the current state of understanding. *Org. Geochem.* **2018**, *123*, 1–16.
- Borjigin, T.; Lu, L.; Yu, L.; Zhang, W.; Pan, A.; Shen, B.; Wang, Y.; Yang, Y.; Gao, Z. Formation, preservation and connectivity control of organic pores in the Sichuan Basin. *Pet. Explor. Dev.* **2021**, *48*, 687–699. [[CrossRef](#)]

13. Gareth, R.; Chalmers, R.; Marc, B.; Ian, M.P. Characterization of gas shale pore systems by porosimetry, pycnometry, surface area, and field emission scanning electron microscopy/transmission electron microscopy image analyses: Examples from the Barnett, Woodford, Haynesville, Marcellus, and Doig units. *AAPG Bull.* **2012**, *96*, 1099–1119.
14. Wang, Y.; Liu, L.; Cheng, H. Gas adsorption characterization of pore structure of organic-rich shale: Insights into contribution of organic matter to shale pore network. *Nat. Resour. Res.* **2021**, *30*, 2377–2395. [[CrossRef](#)]
15. Li, Y.; Hu, Z.; Liu, X.; Cai, Z.; Mu, Y.; Zhang, Q.; Zeng, S.; Guo, J. The pore structure characteristics of deep shale in Longmaxi Formation of Luzhou area. *Fault Block Oil Gas Field.* **2022**, *29*, 584–590.
16. Liu, X.; Zhang, X.; Zeng, X.; Cheng, D.; Ni, H.; Li, C.; Yu, J.; Hu, F.; Li, C.; Wei, B. Pore structure characterization of shales using SEM and machine learning-based segmentation method. *J. China Univ. Pet.* **2022**, *46*, 23–33.
17. Wang, Z.; Jiang, Y.; Fu, Y.; Lei, Z.; Xu, C.; Yuan, J.; Wen, R.; Wang, Z.; Gu, Y.; Yin, X. Characterization of pore structure and heterogeneity of shale reservoir from Wufeng Formation-Sublayers Long-1₁ in Western Chongying based on nuclear magnetic resonance. *Earth Sci.* **2022**, *47*, 490–504.
18. Liu, E.; Liu, C.; Shi, D.; Wang, Y.; Zhu, D.; Xu, Q. Characterization and controlling factors of pore structural heterogeneity of mudstone: A case of upper Paleozoic in northeast Zhoukou Depression, Southern North China Basin. *J. Cent. South Univ.* **2022**, *53*, 3773–3790.
19. Yang, Y.; Wang, K.; Zhang, L.; Sun, H.; Zhang, K.; Ma, J. Pore-scale simulation of shale oil flow based on pore network model. *Fuel* **2019**, *251*, 683–692. [[CrossRef](#)]
20. Mahjour, S.K.; Faroughi, S.A. Selecting representative geological realizations to model subsurface CO₂ storage under uncertainty. *Int. J. Greenh. Gas Control* **2023**, *127*, 103920. [[CrossRef](#)]
21. Li, D.; Bian, C.; Guo, B.; Zeng, X.; Liang, S. Pore structure and reservoir physical properties for effective development of tight sandstone gas: A case study from the Central Sichuan Basin, China. *Geol. J.* **2022**, *57*, 2497–2510.
22. Li, Y.; Zhou, A.; Xie, W.; Qiu, X.; Dai, Y.; Hu, X.; Cheng, X.; Jiang, Y.; Fu, Y.; Wang, Z. Lithofacies division and main controlling factors of reservoir development in Wufeng Formation-Long'sub-member shale in the Luzhou region, South Sichuan Basin. *Nat. Gas Ind.* **2022**, *42*, 112–123.
23. Zhou, A.; Xie, W.; Qiu, X.; Wu, W.; Jiang, Y.; Dai, Y.; Hu, X.; Yin, X. On Exploration and Development Potential of Shale Gas in Longyi₁⁴ Sub-bed in Luzhou Block. *Spec. Oil Gas Reserv.* **2022**, *29*, 20–28.
24. Jiang, C.; Zhang, H.; Zhou, Y.; Gan, H.; Pu, J.; Jiang, Y.; Fu, Y.; Gu, Y.; Li, M.; Wang, Z.; et al. Palaeogeomorphic characteristics of Wufeng-Longmaxi formation and its influence on development of high-quality shale in Dazu area, Western Chongqing. *J. Cent. South Univ.* **2022**, *53*, 3628–3640.
25. Ma, X. Enrichment laws and scale effective development of shale gas in the southern Sichuan Basin. *Nat. Gas Ind. B* **2019**, *6*, 240–249. [[CrossRef](#)]
26. Ma, X.; Xie, J.; Yong, R.; Zhu, Y. Geological characteristics and high production control factors of shale gas reservoirs in Silurian Longmaxi Formation, southern Sichuan Basin, SW China. *Pet. Explor. Dev.* **2020**, *47*, 841–855. [[CrossRef](#)]
27. Zhang, L.; Guo, J.; Tang, H.; Liu, J.; Li, Q.; He, J. Pore structure characteristics of Longmaxi shale in the southern Sichuan Basin. *Nat. Gas Ind.* **2015**, *35*, 22–29.
28. Liu, K.; Ostadhassan, M.; Kong, L. Multifractal characteristics of Longmaxi shale pore structures by N₂ adsorption: A model comparison. *J. Pet. Sci. Eng.* **2018**, *168*, 330–341. [[CrossRef](#)]
29. Xiong, Y.; Zhou, S.; Jiao, P.; Yang, M.; Zhou, J.; Wei, W.; Cai, J. Fractal analysis of micropore structures in coal and shale based on low-temperature CO₂ adsorption. *Nat. Gas Geosci.* **2020**, *31*, 1028–1040.
30. Panigrahy, C.; Seal, A.; Mahato, N.K.; Bhattacharjee, D. Differential box counting methods for estimating fractal dimension of gray-scale images A survey. *Chaos Solitons Fractals* **2019**, *126*, 178–202. [[CrossRef](#)]
31. Pfeifer, P.; Avnir, D. Chemistry in noninteger dimensions between two and three. I. Fractal theory of heterogeneous surfaces. *J. Chem. Phys.* **1983**, *79*, 3558–3565. [[CrossRef](#)]
32. Silva, P.M.; Florindo, J.B. A statistical descriptor for texture images based on the box counting fractal dimension. *Phys. A* **2019**, *528*, 121469. [[CrossRef](#)]
33. Zhang, Y.; Liu, J.; Xu, H.; Niu, X.; Qin, G.; Cao, D. Comparison between pore structure and fractal characteristics of continental and transitional coal measures shale: A case study of Yan'an and Taiyuan formations at the northeastern margin of Ordos Basin. *Acta Pet. Sin.* **2017**, *38*, 1036–1046.
34. Thommes, M.; Kaneko, K.; Neimark, A.V.; Olivier, J.P.; Reinoso, F.R.; Jean, R.J.; Sing, K.S.W. Physisorption of gases, with special reference to the evaluation of surface area and pore size distribution (IUPAC Technical Report). *Pure Appl. Chem.* **2015**, *87*, 1051–1069. [[CrossRef](#)]
35. Zhu, B.; Meng, J.; Pan, R.; Song, C.; Zhu, Z.; Jin, J.; Zhang, C.; Liu, L.; Xu, L.; Zhou, X. Multi-scale characterization of organic matter pore space in deep marine shale combined with mathematical morphology. *Geenergy Sci. Eng.* **2023**, *223*, 211539. [[CrossRef](#)]
36. Zhou, X.; Cuo, W.; Li, X.; Zhang, X.; Liang, P.; Yu, J. Mutual relation between organic matter types and pores with petrological evidence of radiolarian siliceous shale in Wufeng-Longmaxi Formation, Sichuan Basin. *J. China Univ. Pet.* **2022**, *46*, 12–22.
37. Zhu, Y.; Chen, G.; Liu, Y.; Shi, X.; Wu, W.; Luo, C.; Yang, X.; Yang, Y.; Zou, Y. Sequence stratigraphy and lithofacies paleogeographic evolution of Katian Stage-Aeronian Stage in southern Sichuan Basin, SW China. *Pet. Explor. Dev.* **2021**, *48*, 974–985. [[CrossRef](#)]
38. Xu, L.; Meng, J.; Pan, R.; Yang, X.; Sun, Q.; Zhu, B. Sequence stratigraphy and implications for shale gas exploration in the Southern Sichuan Basin, South China. *J. Mar. Sci. Eng.* **2023**, *11*, 1393. [[CrossRef](#)]

39. Xu, L.; Pan, R.; Hu, H.; Meng, J. Contribution of various shale components to pore system: Insights from attributes analysis. *J. Mar. Sci. Eng.* **2023**, *11*, 1327. [[CrossRef](#)]
40. Wang, P.; Jiang, Z.; Ji, W.; Zhang, C.; Yuan, Y.; Chen, L.; Yin, L. Heterogeneity of intergranular, intraparticle and organic pores in Longmaxi shale in Sichuan Basin, South China: Evidence from SEM digital images and fractal and multifractal geometries. *Mar. Pet. Geol.* **2016**, *72*, 122–138. [[CrossRef](#)]
41. Liu, S.; Ma, W.; Luba, J.; Huang, W.; Zeng, X.; Zhang, C. Characteristics of the shale gas reservoir rocks in the Lower Silurian Longmaxi Formation, East Sichuan basin, China. *Energy Explor. Exploit.* **2013**, *31*, 187–219. [[CrossRef](#)]
42. Lyu, P.; Meng, J.; Pan, R.; Yi, X.; Yue, T.; Zhang, N. Characteristics and differences analysis for thermal evolution of Wufeng-Longmaxi shale, Southern Sichuan Basin, SW China. *Minerals* **2022**, *12*, 906. [[CrossRef](#)]
43. Jiang, Z.; Li, X.; Wang, X.; Wang, G.; Qiu, H.; Zhu, D.; Jiang, H. Characteristic differences and controlling factors of pores in typical South China shale. *Oil Gas Geol.* **2021**, *42*, 41–53.
44. Jia, T.; Zhang, S.; Tang, S.; Wang, M.; Xin, D.; Zhang, Q. Characteristics and evolution of low-rank coal pore structure around the first coalification jump: Case study in Southeastern Junggar Basin. *Nat. Resour. Res.* **2022**, *31*, 2769–2786. [[CrossRef](#)]
45. Miao, Y.; Li, X.; Lee, J.; Zhou, Y.; Liu, S.; Chang, Y.; Wang, S. Characterization of hydrocarbon/pores generation and methane adsorption in shale organic matter. *Pet. Sci. Technol.* **2018**, *36*, 1187–1193.
46. Guo, X.; Hu, D.; Huang, R.; Wei, Z.; Duan, J.; Wei, X.; Fan, X.; Miao, Z. Deep and ultra-deep natural gas exploration in the Sichuan Basin: Progress and prospect. *Nat. Gas Ind. B* **2020**, *7*, 419–432. [[CrossRef](#)]

Disclaimer/Publisher’s Note: The statements, opinions and data contained in all publications are solely those of the individual author(s) and contributor(s) and not of MDPI and/or the editor(s). MDPI and/or the editor(s) disclaim responsibility for any injury to people or property resulting from any ideas, methods, instructions or products referred to in the content.